**ORIGINAL PAPER**

# "Evaluation of an electromagnetically actuated drum brake concept"

Lennart Guckes[1] · Jens Hoffmann[2] · Malte Schrimpf[1] · Hermann Winner[1]

**Abstract**

In publications and conferences on the subject of wheel brakes, different concepts of electromechanically actuated wheel brakes can be found, as well as investigations into their suitability for the use in passenger cars. The vast majority of these brakes are disc or drum brakes, which are actuated by an electric motor. In the present publication, a brake concept is considered, that combines an electromagnetically actuated full-pad disc brake with a 10″ duo-duplex drum brake. The brake concept is researched in a project regarding brakes for autonomous shuttles and thus dimensioned using vehicle data of an example shuttle. The electromagnet was designed using finite element methods and the overall brake prototypically realized. The validation of the system design is carried out in component and system tests. The results show the suitability of the concept for the selected vehicle in terms of dynamics, installation space and energy requirements. However, there is a strong dependence of the braking torque output on the frictional sliding speed. Using hypothesis-based testing, electromagnetic effects like eddy currents are ruled out as a possible cause and the friction coefficient within the full-pad disc brake is identified as the main cause for the loss in torque. Consequently, the associated development conflict is identified and lies in the double function of the flux-carrying material in the electromagnet, which also acts as a friction partner for the braking disc.

**Keywords** Future brake system · Automotive brakes · Dry brake · Magnetic brake · Drum brake · Disc brake

## 1 Introduction

Three main development trends can currently be identified in the automotive industry. These are autonomous driving, the increasing electrification of the powertrain and the reduction or avoidance of emissions. The combination of these trends generates novel mobility concepts, such as autonomous shuttles [2]. These present an alternative to passenger transport to the classic passenger car and promise a demand-oriented transport solution in urban areas. For the design of chassis systems, these concepts imply a necessity to reevaluate the requirements placed on the systems [7]. For the wheel brake in particular, the following changes result in an especially significant alteration of use cases:

Autonomous driving:

- The human driver is no longer the operator of the vehicle and the components no longer have to be designed for the worst-case use of human drivers.

Electrification:

- The wheel brake now only takes over a fraction of the braking operations, as the regenerative brake takes over the largest number of braking operations, especially in urban traffic at lower speeds [8].

In contrast to modern hydraulic brake systems, even more suitable, smart and highly integrated concepts can be found that offer particular advantages.

In addition to the conventional hydraulic concepts, electromechanical concepts are currently being developed. The

✉ Lennart Guckes
lennart@guckes.org

Jens Hoffmann
jens.hoffmann@h-da.de

Malte Schrimpf
malte.schrimpf@tu-darmstadt.de

Hermann Winner
hermann.winner@tu-darmstadt.de

[1] Institute of Automotive Engineering, Technical University of Darmstadt, Darmstadt, Germany

[2] University of Applied Sciences Darmstadt, Darmstadt, Germany

anticipated advantages of these concepts are the motivation for further research into this type of brake actuation.

## 2 Motivation

The motivation for developing electromechanical wheel brakes lies both in the functional range required for modern vehicles and in efficiency considerations in operation and production.

Electromechanical, dry brake systems ("dry brake-by-wire") promise the following advantages over classic, hydraulic wheel brakes: [14, 16]

- Easier implementation of driver-independent operation and individual control (brake blending, assistance systems)
- Elimination of individual, distributed hydraulic modules and fluid (ESC, vacuum pump, brake booster)
- No necessity for filling and bleeding in final assembly by the manufacturer
- Modular, decentralized design, thus lower risk of total brake system failure (in case of redundant energy supply)

For passenger cars, research and development is primarily pursuing the electromotive actuation concept [16]. In the state of the art, both electric motor-operated disc brakes and drum brakes can be found [4].

In addition to the electric motor as an actuator, the electromagnet is also known in electromechanics. While in the industry some normally closed (NC) safety brakes with electromagnetic actuation can be found [5], only de-energized (NO) wheel brakes are permitted for passenger-carrying vehicles [15] for stability reasons. In series, there are only versions of the so-called Warner-Trailer Brake, which is a duo-servo drum brake with an electromagnetic actuator

(Warner [17]. In contrast to patents from the early twentieth century, e.g. [12], few research publications address the suitability and performance of this type of actuation, although there are some potential advantages over electromotive actuation:

1. An electric motor as an actuator provides a torque-speed characteristic that is opposite to the actual load characteristic for wheel brake actuation. The motor delivers high speeds at low torques, while the load requires small travels and high forces. Conversion, therefore, requires high-ratio gears with many moving parts with large variances in efficiency over service life and sensitivity to a variety of disturbance variables. A holding solenoid, on the other hand, offers high forces and is limited to small displacements due to its design. As a result, it requires less mechanical complexity to convert the actuator's output for brake actuation.
2. The electric motor often used in the BLDC (Brushless Direct Current) motor design [16] requires three controlled phases, i.e. three current sensors and complex transistor circuits, in addition to an angle sensor. A holding solenoid, on the other hand, can operate in a single phase.

## 3 Concept

The wheel brake concept under investigation is based on a patent from the Knott company [11], which was further developed in cooperation with the Department of Automotive Engineering of TU Darmstadt and Continental Teves [1]. It comprises a 10" duo-duplex drum brake (1, Fig. 1), inside which a coaxial holding solenoid (3) is situated. The holding solenoid is attracted to the armature disc (2)
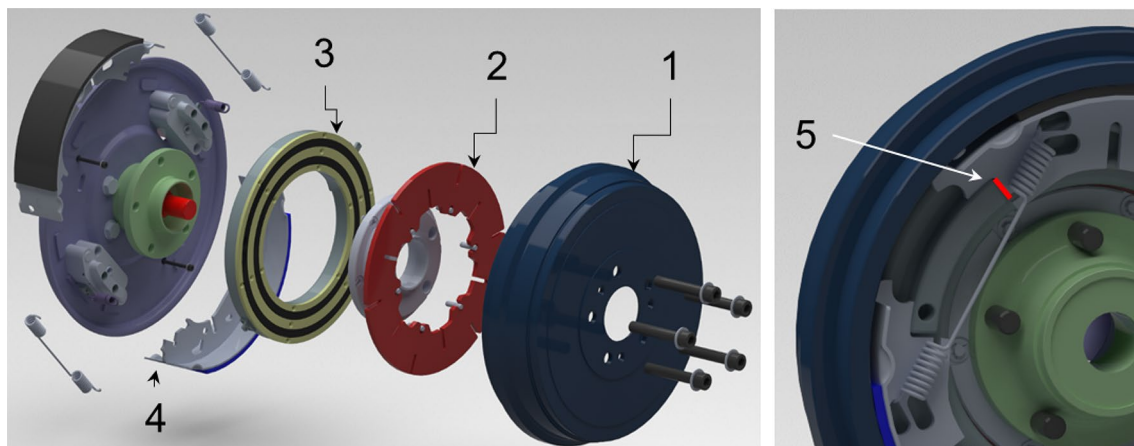


**Fig. 1** 3D views of the hybrid brake concept (1: drum, 2: armature disc, 3: holding solenoid, 4: drum brake shoes, 5: force transmission surface)

rotating with the wheel when the solenoid coils are energized. The frictional torque resulting from the axial magnetic force between the disc brake and solenoid is transmitted as an actuating force to the drum brake shoes (4) via the teeth on the back of the solenoid (5). The concept, therefore, represents a combination of a duo-duplex drum brake in series connection with a magnetically actuated full-pad disc brake. The brake works equally in both directions, as it is designed symmetrically. The system can be powered by a current controller working at 12 Volts. To release the brake, the magnet is pulled against the back plate with return springs, so that the brake is released when no current is applied.

The block diagram (Fig. 2) shows the technical function with the respective state variables.

In detail, the brake actuation process can be described as follows: In the beginning, the brake is in its released state. A current setpoint $I_{set}$ is set for the solenoid coils, which are controlled by a current controller with the control voltage $U_{con}$. The clearance or the initial air gap of the magnetic disc brake is closing as soon as the magnetic force $F_{mag}$ is large enough to overcome the return springs and the solenoid moves toward the disc with its displacement $x_S$. When the holding solenoid attaches to the disc, a friction torque $M_{Di}$ is generated. The friction torque causes the magnetic ring to rotate at a small angle $\varphi_S$ and the tangential force $F_{tan}$ is transmitted to the actuation surfaces of the drum brake shoes. This force is used to actuate the brake shoes which generate a friction torque $M_{Dr}$ at the drum.

For testing purposes, the prototype can be configured in different setups:

1. System setup: disc and drum brake (as shown in Fig. 2)
2. Disc setup: disc brake only

## 4 Dimensioning of the wheel brake

The wheel brake is designed for a rear wheel of an autonomous shuttle, in particular, the so-called "CUbE" from Continental [2]. The shuttle itself is designed to have a preferred driving direction because it would otherwise require a complex cooling system working in all driving directions. The case of an emergency braking procedure with a deceleration of $a = -1g$ on a high friction coefficient requires a braking torque of approximately 1100Nm at the rear wheel. The dimensioning of the concept is based on this value.

The total braking torque is calculated according to Fig. 2:

$$M_{Br} = M_{Dr} + M_{Di} = \frac{M_{Di}}{r_{act}} \cdot r_{Dr} \cdot c^* + M_{Di} = M_{Di} \left( \frac{r_{Dr}}{r_{act}} \cdot c^* + 1 \right)$$
$$= F_{mag} \cdot \mu_{Di} \cdot r_{eff} \cdot \left( \frac{r_{Dr}}{r_{act}} \cdot c^* + 1 \right)$$
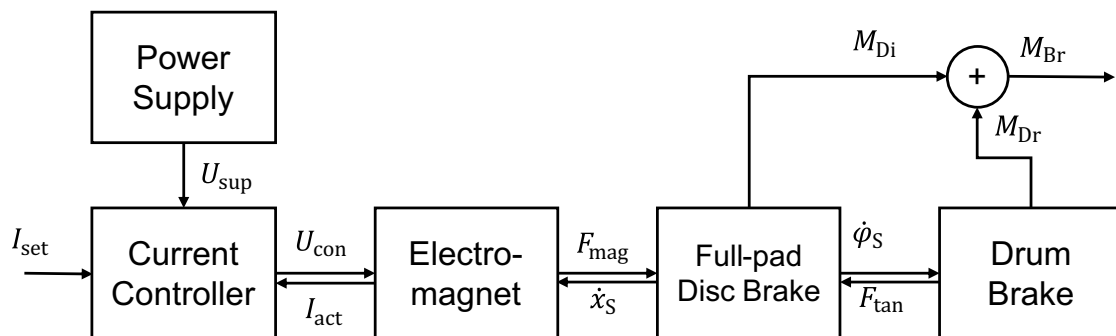
The necessary actuator force is calculated:



**Fig. 2** Block diagram of the hybrid brake concept

**Table 1** Assumptions and values for dimensioning

| $M_{Br}$ | Total braking torque | 1100 Nm |
|---|---|---|
| $\mu_{Di}$(assumed) | Friction coefficient on disc | 0.3 |
| $r_{eff}$(assumed) | Effective friction radius on disc | 0.1 m |
| $r_{Dr}$ | Friction radius on drum surface | 0.127 m |
| $r_{act}$ | Actuation radius of drum brake shoes | 0.09 m |
| $c^*$(assumed) | Brake factor of drum brake | 2.5–4.6 (with $0.3 < \mu_{Dr} < 0.4$) |

$$F_{\mathrm{mag}} = \frac{M_{\mathrm{Br}}}{\mu_{\mathrm{Di}} \cdot r_{\mathrm{eff}} \cdot \left( \frac{r_{\mathrm{Dr}}}{r_{\mathrm{act}}} \cdot c^* + 1 \right)}$$

The following design variables are estimated or determined geometrically (Table 1):

The calculated necessary magnetic force lies therefore between $F_{\mathrm{mag}}(c^* = 2, 5) = 8\mathrm{kN}$ and $F_{\mathrm{mag}}(c^* = 4, 6) = 5\mathrm{kN}$.

The torque share of the disc brake to the total torque is calculated as follows:

$$\frac{M_{\mathrm{Di}}}{M_{\mathrm{Br}}} = \frac{1}{\frac{r_{\mathrm{Dr}}}{r_{\mathrm{act}}} \cdot c^* + 1}$$

The equation yields the values $\frac{M_{\mathrm{Di}}}{M_{\mathrm{Br}}}(c^* = 2, 5) = 0, 22$ and $\frac{M_{\mathrm{Di}}}{M_{\mathrm{Br}}}(c^* = 4, 6) = 0, 14$. Since the drum and armature disc
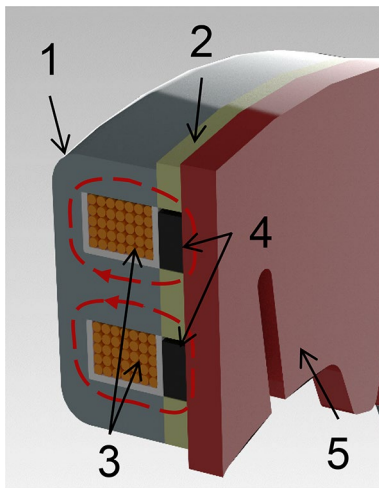


**Fig. 3** Cross section of the holding solenoid (1: steel yoke, 2: cast friction rings, 3: copper coils, 4: NAO friction material, 5: steel armature disc, magnetic flux in red)

have the same angular velocity, the power contribution of the armature disc to the total frictional braking power is also $14 - 22\%$.

## 5 Actuator

A holding solenoid, which works at minimal airgaps, is used as the actuator, which consists of multiple individual parts (Fig. 3).

The cross-section and the choice of materials are the results of a student thesis [6], with the aim to optimize the magnetic force yield in the available installation space by means of FEM calculations. The parts carrying the magnetic flux are the steel yoke with "E" cross-Sect. (1), the cast friction rings (2) and the armature disc made of steel (5). In addition, two excitation coils (3) are inserted as well as two friction rings made of a metal-free NAO friction material (4). The two excitation coils carry currents in different directions so that the resulting flux is amplified. In the event of failure of one coil, the brake can still be operated, but with lower maximum torque if they are connected in parallel.

Table 2 gives an overview of the functions of each component.

The cast friction rings were chosen as a compromise between high saturation flux density (about 1,5 T) and graphite content (about 3,5%) of the material. For production purposes, they were designed with a thickness of 4 mm.

## 6 Testing

### 6.1 Testing method

To investigate the suitability of the brake, different tests are carried out to validate the design.

**Table 2** Functional overview of the components of the holding solenoid

| Part | Name | Functions |
|------|------|-----------|
| 1 | Steel yoke | 1. Guidance of magnetic flux with high permeability |
|  |  | 2. Enclosure and containment of all components of the holding solenoid |
|  |  | 3. Transmission of the tangential forces generated by friction to actuate the drum brake shoes |
| 2 | Cast friction rings | 1. Guidance of magnetic flux with high permeability |
|  |  | 2. Lubrication of the friction surface by means of embedded graphite spheres |
|  |  | 3. Generation of the friction torque in combination with disc |
| 3 | Copper coils | Generation of the necessary excitation for the magnetic flux |
| 4 | NAO—friction rings | Improvement of the friction properties of the ring and armature plate pairing |
| 5 | Armature disc | 1. Guidance of magnetic flux with high permeability |
|  |  | 2. Friction partner for holding solenoid |
|  |  | 3. Transmission of the braking torque to the wheel |

1. The actuator itself is examined for the actuator force it can generate.
2. The dynamics for the actuation of the brake are identified.
3. The generated torque at the disc is identified as well as the total braking torque at different speeds.

Any deviations found from the design assumptions are then investigated and evaluated for their cause using hypothesis-based tests.

The respective testing procedures are documented in the following test descriptions.

## 6.2 Experiments to identify the generated actuator force

### 6.2.1 Goal

The aim of the experiment is to identify the actuator force that can be generated as a function of the air gap present, to examine the actuator for compliance with the requirements ($F_{mag}(c^* = 2, 5) = 8kN$). In addition, the electrical power loss at the required current is calculated.

### 6.2.2 Test execution

The achieved magnetic force of the solenoid is identified quasi-statically by means of pull-off tests since a direct force measurement between the ring and disc is not applicable without influencing the magnetic flux. For this purpose, the ring and disc are mounted on a tensile force testing machine and quasi-statically pulled off under constant current flow. The required electrical voltage is also considered for power calculation. The highest tensile force measured in each case during the pull-off process is used as the passing criterion to check whether the actuator has reached its target force. To simulate different constant air gaps, brass foils with defined thicknesses $d = [0; 0, 1; 0, 25; 0, 35]$mm are placed between the holding solenoid and the armature disc. These have a relative magnetic permeability similar to vacuum with $\mu_R \approx 1$. For each data point in the evaluation one measurement was taken.

### 6.2.3 Evaluation

The actuator achieves a maximum force of 7.8 kN with the smallest possible air gap and 20 A current and thus reaches the required actuator force with a negligible 200 N difference (Fig. 4). The electrical resistance of the windings connected in series is $R_{ov} = 0, 54\Omega$ at room temperature. Thus, the electrical power at a current of 20 A results in $P_{el} = R \cdot I^2 = 216$W. The force curve at the smallest possible air gap shows the typical curve of a holding solenoid operated up to saturation. For larger air gaps, the relationship between force and Resembles a linear curve more closely, which suggests that the solenoid is in the lower, linear flux density range.

## 6.3 Test for evaluation of system dynamics and ABS suitability

### 6.3.1 Goal

The system dynamics of the hybrid brake are tested in the System Setup on a test bench to investigate the brake concept's suitability for slip control at an early prototype stage.

### 6.3.2 Execution

The brake is controlled by means of jumps in the setpoint value. At a vehicle speed of constant 9 km/h, the solenoid is exposed to voltage jumps from 0 to 12 V and vice versa.
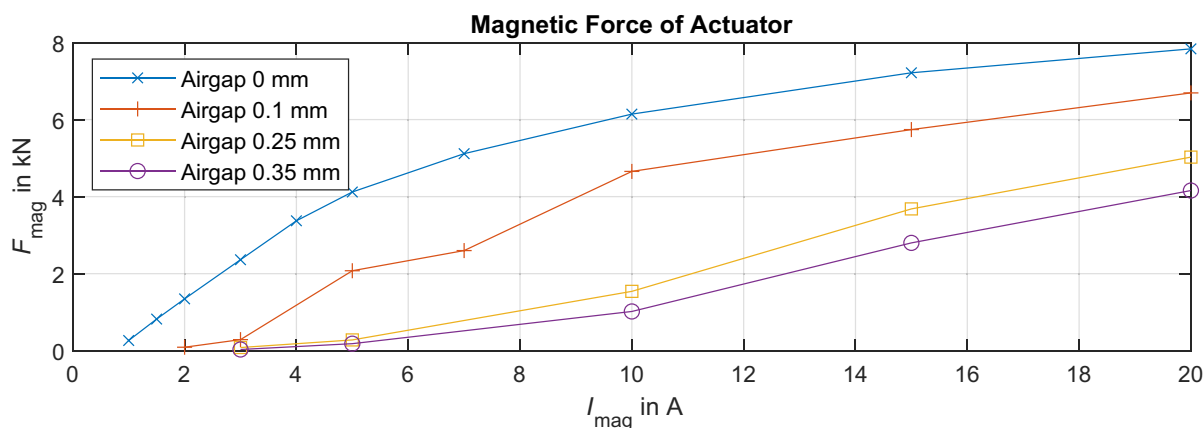


**Fig. 4** Measured holding force over current and air gap

To reduce the influence of random measurement deviations, the measurements are repeated three times. A measurement frequency of 10 kHz is chosen, to get a sufficient resolution on the torque response.

### 6.3.3 Evaluation

The times taken to reach 90% of the final torque are used for evaluation. For this purpose, segments are formed from the measured data, each of which is consisting of either "voltage jump rising" and "voltage jump falling". Within these segments, the duration is calculated which is required to reach 90% of the final torque within the segment from the time of the voltage step (Fig. 5).

It can also be seen, that the torque is oscillating. The oscillation is most likely caused by a stick–slip effect, as the solenoid sticks and slips on the armature disk. This effect can cause NVH issues with the brake, that are not researched further in this article.

The times achieved averaged over the three repetitions for the group "voltage jump rising" result in: $\tau_{90} = 54$ms and for "voltage jump falling": $\tau_{90} = 57$ms.

For a fast change in torque, this results in a maximum possible frequency of $f = \frac{1}{\tau_{90}} \approx 17,6$Hz. For modern slip controllers, which control in the range up to 10 Hz in hydraulic brake systems [9], the brake can thus be considered suitable, since it can be applied with a higher frequency.

## 6.4 Tests on the torque generation of the overall system and the disc brake

For the identification of the generated torques, tests of the entire system (system setup) as well as only of the solid disc brake (disc setup) are carried out.

### 6.4.1 Goal

The goal of the test is to identify the braking torque generated from the disc brake subsystem and in the overall disc and drum system as a function of the variables current and speed.

### 6.4.2 Execution

To identify the torque generation, a map with different speeds and current strengths is created and individual points of this map are tested in a stationary manner (by means of drag braking) on a brake dynamometer.

The speeds considered are $v = [2;5;15;30;55;100;144]$km/h or $v = [0, 5;1, 3;4, 1;15, 3;27, 8;40]$m/s with a wheel diameter of $0, 3$m and the currents $I = 1..14$A in steps of 1A. To reduce the influence of random measurement deviations, the measurements are repeated three times in disc brake mode.

### 6.4.3 Evaluation

The evaluation of the tests is automated according to the following procedure (Fig. 6):

1. Filtering of torque and current signal by a two-sided moving average.
2. After reaching 97% of the nominal current, the maximum torque is searched for in a time window of 150 ms. The search period results from the time usually required to reach the maximum braking torque of 150 ms in a vehicle (TTL: Time to lock) [13].
3. The start time for averaging is set to when 95% of the maximum torque found is reached.
4. The end time for averaging is set according to the duration of one complete revolution of the brake. If one revolution is not reached in the test duration (due to the low
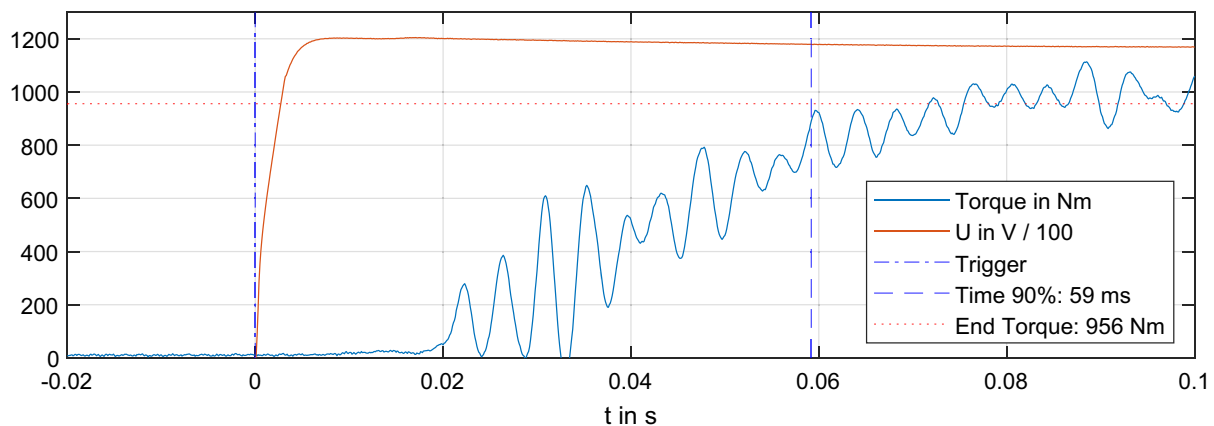


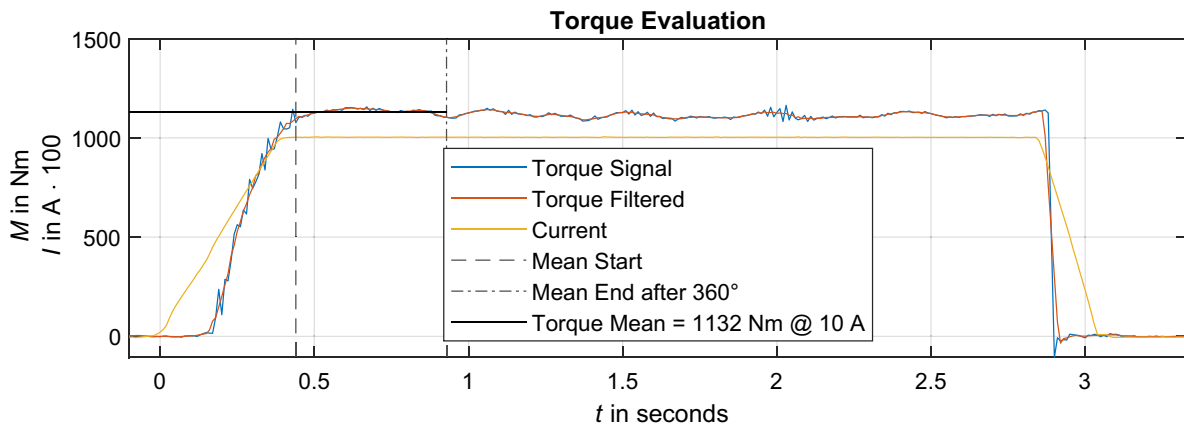**Fig. 5** Evaluation of system dynamics for time to reach 90% of final torque

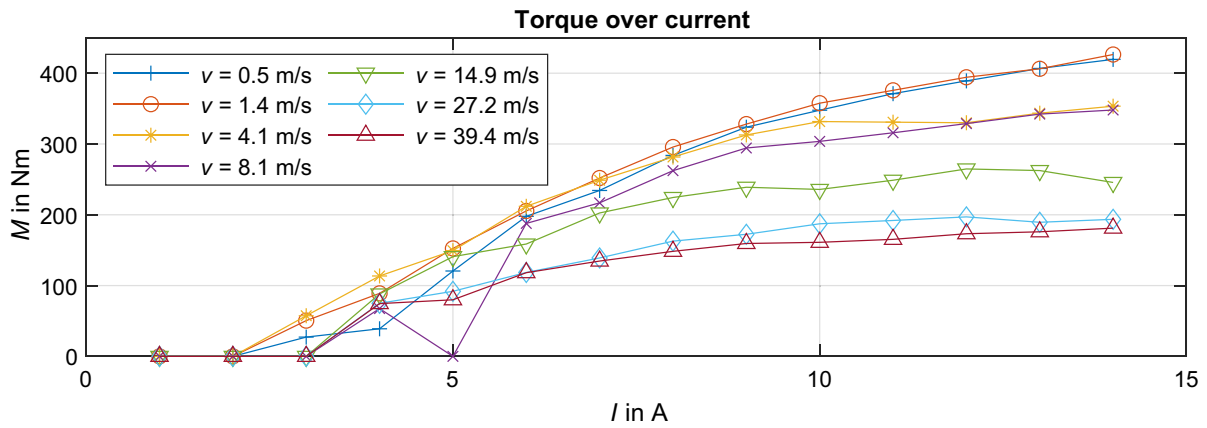**Fig. 6** Evaluation of one drag braking test



**Fig. 7** Torque generation of the disc brake as a function of the current
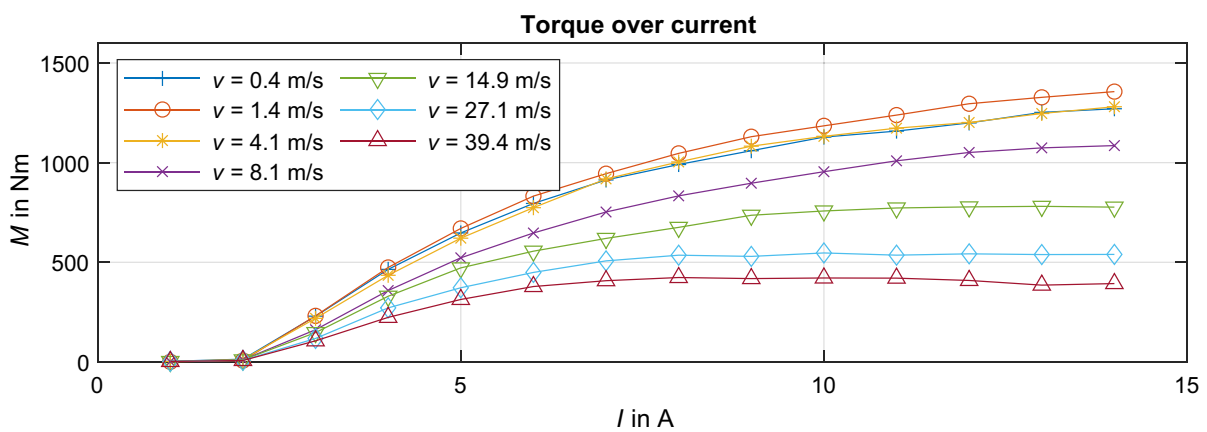


**Fig. 8** Torque generation in system setup over current

velocity), the end time is set to when the current drops below 97% of the set current.

By limiting the evaluation duration to one revolution, the disturbance variable influence of the temperature during the measurement is reduced.

For evaluation purposes, the achieved torques are plotted in curve arrays versus current and versus velocity for both the disc brake (Fig. 7) and the overall system (Fig. 8).

The following expected characteristics are included in the curve over the current for the disc brake (Fig. 7):

1. As the current increases, the torque increases as a result of the higher axial force in the disc brake.
2. Due to saturation of the flux density in the flux path, the increase in torque is degressive.
3. In the range of approx. 1–2 A, no torque is generated. The reason for this is the necessity to overcome the

initial air gap between yoke and armature disc, which requires a minimum axial force defined by the return springs.

As the disc brake generates the actuation force for the drum brake, these characteristics are also observable in the torque curves for operation in the system setup (Fig. 8).

However, when considering the torque curve over the velocities, an unexpected behavior occurs. At all current levels, a dependence of the torque on the speed can be observed. At the highest current level, the percentage decrease in torque in disc mode between slow and fast driving is 58%. In system setup, this decrease amounts to 71%. This is particularly clear from the plot of torque versus velocity (Figs. 9 and 10).

With the two torque curves, the effective $c^*$ can be calculated using the equation for the torque ratio:
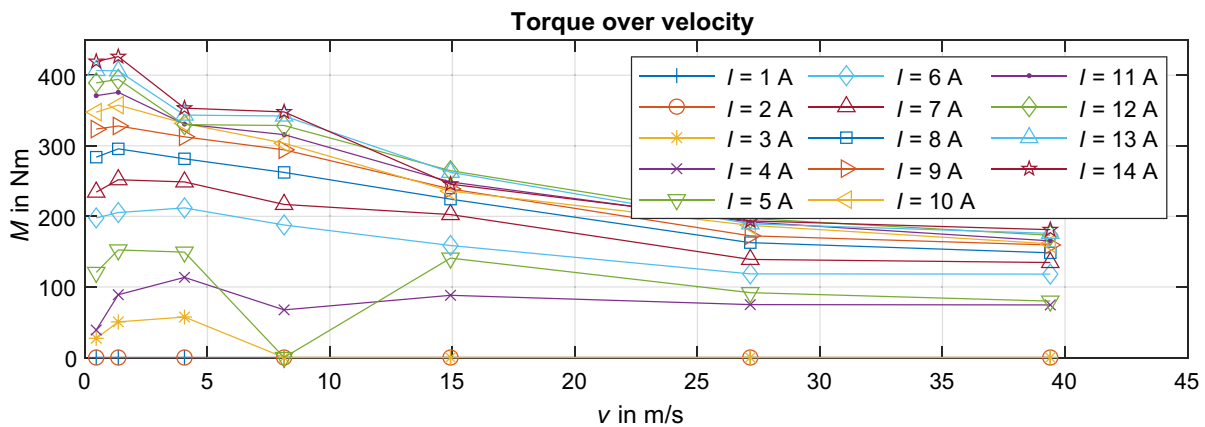


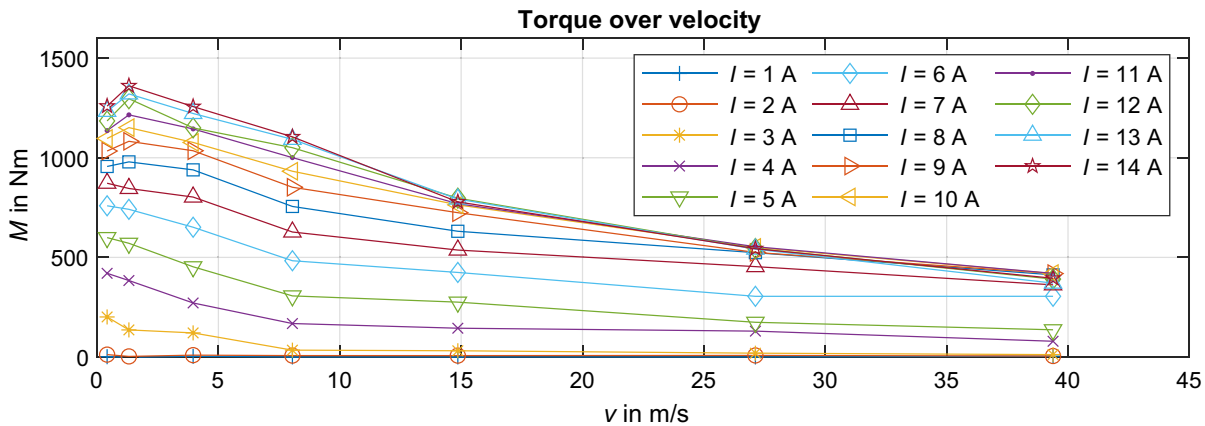**Fig. 9** Torque generation of the disc brake over velocity



**Fig. 10** Torque generation in system setup over velocity

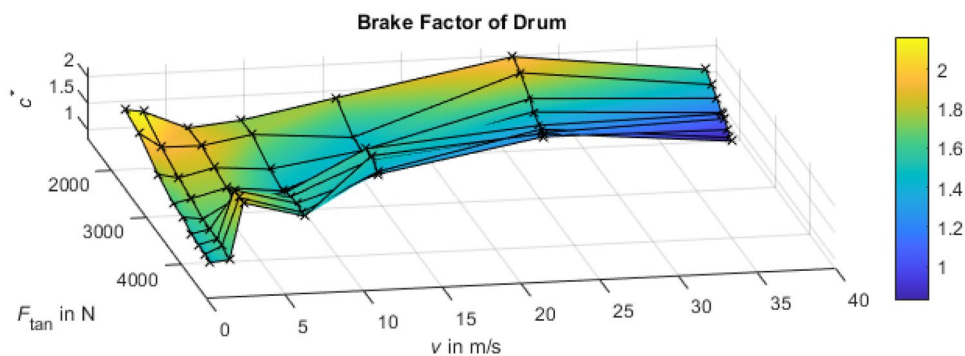**Fig. 11** Calculated brake factor c* for the drum brake



**Table 3** Geometric values of drum brake for brake factor calculation

| | |
|---|---|
| $a = 93$mm | Vertical distance of pivot to center |
| $c = 20$mm | Horizontal distance of pivot to center |
| $r = 127$mm | Radius of drum |
| $\alpha = 76° \cong 1,33$ | Angle of coverage of brake pad on brake shoe |

$$c^* = \left(\frac{M_{Br}}{M_{Di}} - 1\right) \cdot \frac{r_{act}}{r_{Dr}}$$

The brake factor $c^*$ is represented via the calculated actuation force $F_{tan} = \frac{M_{Di}}{r_{act}}$ and the velocity (Fig. 11).

It can be seen from the diagram that the brake factor of the drum brake lies between $c^* = 0,83$ and $2,16$ The value is particularly low in the range of high speeds and high actuating forces, and higher at low speeds and lower actuating forces. The calculated value based on the measured data is therefore lower than the design assumption made in Table 1.

With the calculated brake factors it is possible to calculate the friction coefficient between the drum and the brake shoes $\mu_{Dr}$ using the following formula for two leading brake shoes in a drum brake [3]:

$$c^* = \frac{2\mu_{Dr}h}{K_1 a_0 - r\mu_{Dr}}, \mu = \frac{K_1 a_0 c^*}{2h - rc^*}$$

$$K_1 = \frac{\sin(\alpha) + \alpha}{4 \cdot \sin\left(\frac{1}{2}\alpha\right)}; a_0 = \sqrt{a^2 + c^2}$$

With the following geometric values for the drum (Table 3).

The results of the calculation are shown in Fig. 12:

The friction coefficient of the drum brake $\mu_{Dr}$ varies between 0.29 and 0.15.

To investigate the cause of the unexpected decrease in torque at higher speeds, especially in disc operation, two hypotheses are set up and falsification tests based on them are carried out. The loss in torque of the drum brake itself will not be researched further, as the disc brake component represents the center of interest for the braking concept.

Hypothesis 1: The drop in torque is due to a decreasing axial force over velocity due to magnetic field weakening (due to eddy currents or mechanically induced air gap fluctuations)
Hypothesis 2: The drop in torque is due to a speed-dependent coefficient of friction between the solenoid and the armature disc

**Fig. 12** Calculated friction coefficient $\mu_{Dr}$ of drum brake
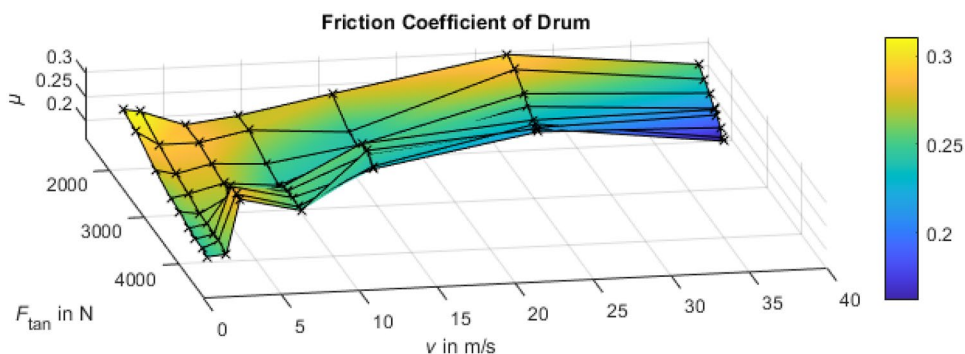
### 6.5 Falsification tests for hypothesis 1: magnetic field weakening during operation

The underlying hypothesis assumes a weakening of the magnetic force during operation as a function of the rotational speed. The magnetic force of an electromagnet largely depends on the flux density $B$, the flux-carrying area $A$ and the permeability in the air gap $\mu_0$. Maxwell's formula of magnetic traction force [10], p. 74) shows this relationship:

$$F_{\mathrm{mag}} = \frac{B^2 A}{2\mu_0}$$

The effective flux density in the prototype is influenced by the size of the air gap present, by eddy currents arising which counteract the flux density, and by saturation effects in the material through which the flux flows. Eddy currents occur when there is a change in flux density in the electrically conducting material. The necessary potential difference arises from the induced voltage $U_{\mathrm{ind}}$, which is proportional to the change in flux density $\dot{B}$ in the material. However, if the geometry of the prototype is considered ideally, no change in the flux density can be assumed, since the flux does not change under rotation of the armature disc, i.e., when considered over the circumference. The same applies to the radial flux profile. In reality, however, there can be deviations in the centric arrangement between the solenoid and the armature disc, which can cause a radial flux density change in the disc.

A second chain of effects to weaken the flux density would be an increase of the mean air gap when the brake is applied depending on the rotational speed, which would be due to dynamic effects. If one of these phenomena were to weaken the magnetic flux density, in this case saturation would have to occur only at a higher excitation (at a higher current).

The investigation of the torque of the disc brake (Fig. 7) shows a typical saturation curve of the flux density in the materials of the magnetic circuit. If there was a field weakening effect in the area of higher speeds this saturation would shift to higher excitations (meaning higher currents). Figure 13 shows the torque curve over currents in a normalized display, by dividing all torque values of each velocity with the torque value at 14 A. The graph shows that each curve has its point of inflection in the range of 7 to 8 A. This observation consequently argues against the hypothesis of a field weakening effect.

To be able to make a more substantiated statement about the effective magnetic force, the change in flux density is identified via the induced voltage in a further experiment using several measuring coils introduced into the flux path of the solenoid.

#### 6.5.1 Experiments to identify the effective magnetic flux density

**6.5.1.1 Goal** The aim of the experiment is to identify the effective magnetic flux density at different currents and speeds and thus to estimate the axial force in the disc brake system.

**6.5.1.2 Execution** For the experiment, fixed speeds are approached with the dyno test bench with $v = [2;10;15;20;40]$ m/s and fixed currents of $I = [8;12;16;20]$ A are set. After reaching the set velocity, the induced voltages of the measuring coils are recorded during the actuation and release of the brake for a measurement period of 2 s. The voltage of the measuring coils is measured and then integrated to calculate the static flux density at a fixed current and velocity.
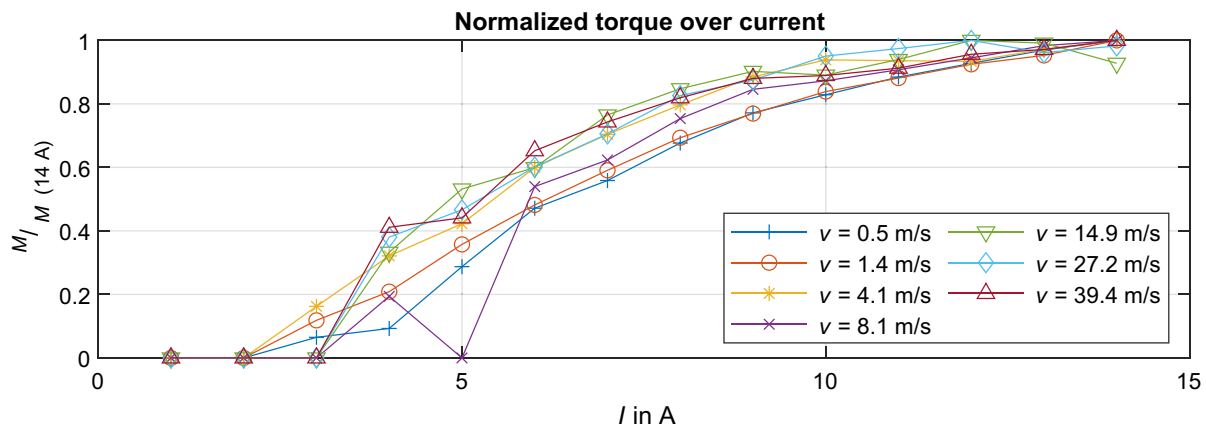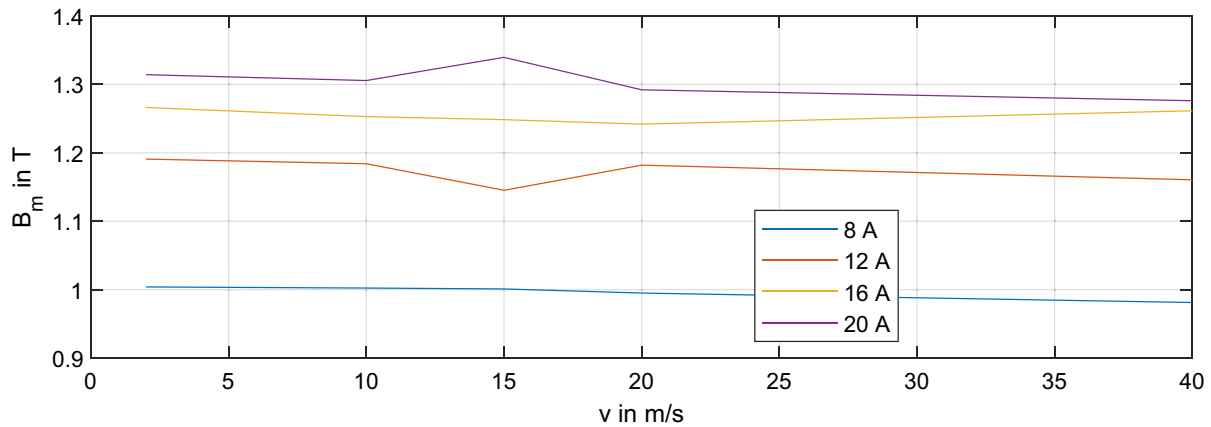


**Fig. 13** Normalized torque curve for the disc brake

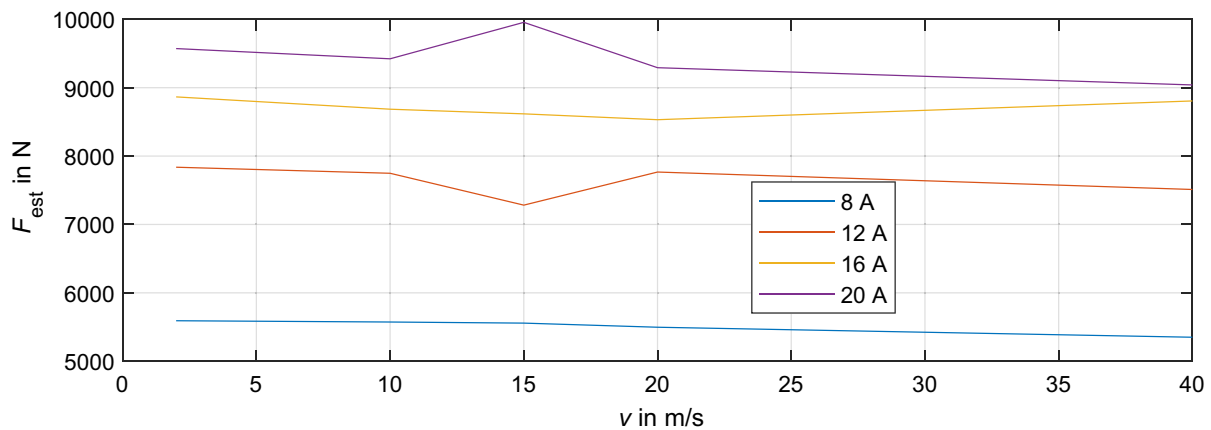**Fig. 14** Flux densities over wheel circumference velocity



**Fig. 15** Actuator force estimation based on the calculated flux density

**6.5.1.3 Evaluation** The series of experiments yields the following flux densities versus velocity. Figure 14 shows the flux density over the center leg of the solenoid.

Maxwell's formula of magnetic traction force can be used to calculate the acting axial forces considering all three legs of the yoke and to plot them versus velocity (Fig. 15).

The estimated forces of the actuator are consistently higher than the identified pull-off forces of the actuator without measuring coils in Fig. 4, but a direct comparison of the values is not valid due to the deviation in the design of the solenoid, which was necessary to include the measurement coils.

The highest percentage deviation in force between slow and fast speeds can be observed at 20 A and amounts to 5.6%, which is not sufficient to explain the 71% drop in braking torque that was observed earlier. Consequently, the decrease of the friction torque over the velocity does not have its cause in a significant decrease in the magnetic flux density or magnetic force. The hypothesis of field weakening during operation is thus falsified.

## 6.6 Falsification tests for hypothesis 2: "Speed-dependent coefficient of friction between magnet and armature plate"

### 6.6.1 Goal

The aim of the experiment is to identify the coefficient of friction of the armature disc and cast friction rings $\mu_{Di}$ as a function of speed and contact pressure. To do so, it is necessary to know the acting axial force and the resulting circumferential force.
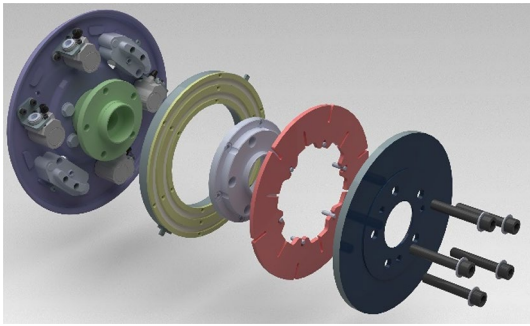
**Fig. 16** Exploded view of the assembly for hydraulic actuation of the yoke ring without friction lining rings

### 6.6.2 Execution

For the execution of the experiments, an adaptation of the design is made. Since the magnetic force in operation can only be estimated by derivation from flux density, the full-pad disc brake is actuated by hydraulic cylinders (see Fig. 16), which provides more precise knowledge of the axial force via the hydraulic pressure. Since the axial tensile force acts only between the cast rings and the armature disc in magnetic operation, the two friction material rings are removed for this experiment. The velocities are set to $v = [2;10;15;20;40]\frac{m}{s}$. The pressure levels are also varied with $p = [5;10;30;55]$bar, which corresponds to the axial forces of $F_{ax} = [1;2;6;11]$kN. To reduce the influence of random measurement deviations, the measurements are repeated three times.

### 6.6.3 Evaluation

The evaluation shows that the coefficient of friction of the cast rings on the armature disc, which are mainly involved

in the friction pairing, drops sharply with speed (Fig. 17). The friction values were calculated assuming a constant effective friction radius and averaged over the three repetitions in each case. For low speeds, friction values in the range $0,37 < \mu_{Di} < 0,67$, are obtained, and in the range of higher speeds only $0,11 < \mu_{Di} < 0,24$, corresponding to a percentage change of 70% and 67%, respectively. The friction values at low speeds are much higher than the ones assumed for the initial dimensioning of the brake. Additionally, a dependency on surface pressure becomes apparent, with higher surface pressure the friction coefficient of the disc brake decreases.

The result of this test shows that the hypothesis of the speed-dependent coefficient of friction cannot be falsified and therefore withstands. Looking ahead, there is the question of the involvement of friction lining rings in friction force generation. This cannot be clarified with this test setup, since in magnetic operation the tensile forces exist only between the armature disc and the cast friction rings, whereas the hydraulic test setup would generate compressive forces over the entire ring.

For the drop of friction coefficient over speed there are different possible explanations. One could have its cause in the temperatures of the friction areas, which could not be measured in the experiments because there was no way to put a temperature sensor at the surface directly. If the temperature of the surface would have reached very high levels, the typical effect of brake fading can occur. The differences in friction coefficient over contact pressure occur due to the compression of the friction partners. For lower contact pressures the unevenness of the two surfaces that are pressed against each other might be higher, than the unevenness with higher contact pressures. A higher unevenness of the surface could have an impact on the friction coefficient of the surfaces.
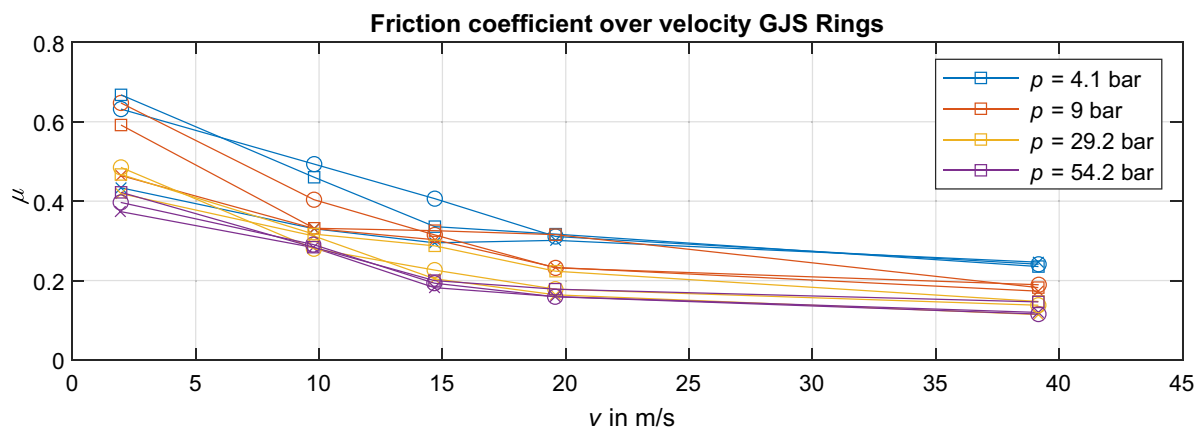


**Fig. 17** Coefficient of friction $\mu_{Di}$ of GJS rings versus speed v, including repetition of measurements marked with x and o

# 7 Conclusion and outlook

Investigations of the magnetic hybrid brake concept show that a high braking torque is generated, especially in the low-speed range, even with low electrical power ($P_{el}$(1350Nm, 14A) = 106W). The dynamics of the brake are not inferior to the state of the art of today's hydraulic systems, and the basic requirements on dynamics for ABS control are met. The design of the brake meets the installation space objective of realizing a complete wheel brake including actuation within a 10-inch drum brake space. The mechanical complexity and number of moving parts are significantly lower than that of similarly powerful, electric motor-actuated drum brake concepts, which rely on multistage, high-ratio transmissions.

However, the existing challenges of the concept are evident in the strong dependence of the generated braking torque of the magnetic disc brake on the speed. After the systematic, deterministic exclusion of influences of the drum brake and of eddy currents or dynamic air gap changes within the magnetic disc brake, the coefficient of friction in combination with the effective friction radius has shown to be the most sensitive parameter depending on the disturbance variable of speed and also contact pressure. This reveals the major development conflict in the material of the yoke of the solenoid, which must have both favorable flux-carrying properties and be a robust friction partner for the rotating armature disc. Furthermore, torque fluctuations occur over time, which can cause NVH problems in the event of resonance.

Due to its design, the wheel brake is limited to the medium to upper range of torques for a braking operation in its control capability since the initial air gap must be overcome with a medium current for application and the solenoid hits the disc as a result of the increase in magnetic force due to a decreasing airgap. After the solenoid has been applied, however, the current can be reduced to subsequently set a lower torque. The suitability of the brake is thus reduced to vehicles that perform comfort braking predominantly by means of an alternative system (e.g. a regenerative brake) and use the hybrid brake for braking with higher torque requirements in hazardous situations. An autonomous, electrified shuttle could be considered as an example.

Looking ahead, further investigation into the suitability of the brake concept linking controllability for low torques with ride comfort is needed. Based on the test results, it is advisable to focus development on the subsystem of the magnetic disc brake to improve its friction behavior. Due to the aforementioned development conflict, an investigation of different materials or coatings to optimize the two functional objectives of flux guidance and friction force generation is recommended.

## Declarations

**Conflict of interest** The research leading to the results was funded by Continental Teves AG & Co. oHG, Rödelheim.

## References

1. Bach, U., Guckes, L., Gädke, M., Stauder, P., Hoffmann, J. and Pla, S.: Trommelbremse für ein drehbares Element. DE102019209523A1. https://depatisnet.dpma.de/DepatisNet/depatisnet?action=bibdat&docid=DE102019209523A1 (2019).
2. Baum, M. (2017), "Continental treibt mit dem Entwicklungsfahrzeug CUbE Technologien für fahrerlose Fahrzeuge voran", available at: https://www.continental.com/de/presse/pressemitteilungen/cube-technologien-74444 (Accessed 11 December 2020).
3. Baumgartner, H., Gerum, E., Pahle, W., Siebke, A., Pehle, M.: Nutzfahrzeugbremsen. In: Breuer, B., Bill, K.H. (eds.) Bremsenhandbuch, pp. 233–259. Springer Fachmedien Wiesbaden, Wiesbaden (2017)
4. Bayer, B., Büse, A., Linhoff, P., Piller, B., Rieth, P.E., Schmitt, S., Schmittner, B., Völkel, J., Zhang, C.: Electro-mechanical brake systems. In: Winner, H., Hakuli, S., Lotz, F., Singer, C. (eds.) Handbook of driver assistance systems: basic information, pp. 731–744. Components and Systems for Active Safety and Comfort, Springer International Publishing, Cham (2016)
5. Chr. Mayr GmbH + Co. KG (2022), "ROBA-stop®-M: Robuste Motorbremse", available at: https://www.mayr.com/de/produkte/bremsen/wellenmontierte-bremsen/roba-stop-m~55 (Accessed 29 Mar 2022).

6.  Guckes, L. (2018), "Systematische analyse und optimierung einer magnetisch aktuierten trommelbremse anhand eines simulationsmodells", Master Thesis, Fachgebiet Fahrzeugtechnik (FZD), Technische Universität Darmstadt, Darmstadt, 2018.

7.  Guckes, L., Winner, H., Hoffmann, J. and Pla, S. (2021), "Requirements and Test Cycles for Brake Systems of Autonomous Vehicle Concepts on the Example of an Autonomous Shuttle", paper presented at Euro Brake, Barcelona, available at: https://www.fisita.com/library/eurobrake/2021/3176eb2021-ibc-006 (Accessed 9 May 2022).

8.  Hoffmann, J. and Wörsdörfer, K.-F. (2020), "End of oversizing: smart designing of brake systems for BEVs". In: Pfeffer, P.E. (Ed), 10th International Munich Chassis Symposium 2019, Proceedings, Springer Fachmedien Wiesbaden, Wiesbaden, p. 595.

9.  Ivanov, V., Savitski, D., Shyrokau, B.: A survey of traction control and antilock braking systems of full electric vehicles with individually controlled electric motors. IEEE Trans. Veh. Technol. **64**(9), 3878–3896 (2015)

10. Kallenbach, E., Eick, R., Ströhla, T., Feindt, K., Kallenbach, M., Radler, O.: Elektromagnete: Grundlagen, Berechnung, Entwurf und Anwendung, 5th edn. Vieweg, Wiesbaden (2018)

11. Klumpner, A., Klumpner, B.: Innenbackenbremse mit elektromagnetischer Betätigungseinrichtung DE102011100088A1. https://depatisnet.dpma.de/DepatisNet/depatisnet?action=bibdat&docid=DE102011100088A1 (2011).

12. Phair, H.: Electromagnetic Friction Apparatus US000002304118A. https://depatisnet.dpma.de/DepatisNet/depatisnet?action=bibdat&docid=US000002304118A (1942).

13. Pinkow, S. (2017), "Continental's cutting-edge brake technology MK C1 enables the next step to highly automated driving", available at: https://www.continental.com/en/press/press-releases/cutting-edge-brake-technology-mk-c1/ (Accessed 8 June 2022).

14. Reichenbach, M.: Wir sind auf dem besten Weg zur trockenen Bremse. ATZ—Automobiltechnische Zeitschrift **124**(6), 22–25 (2022)

15. United Nations (UN) (2018), ECE R13-H.

16. Vey, C., Hoffmann, J., Semsch, M. and Pla, S. (2019), Brakes 2025—design of an electromechanical drum brake, Dresden.

17. Warner Electric (2022), "Anhänger-Radnabenbremsen", available at: https://www.warnerelectric.com/de-DE/products/brake-products/trailer-brakes/trailer-wheel-brakes (Accessed 29 March 2022).